Bulk Photovoltaic Effect in a Pair of Chiral–Polar Layered Perovskite-Type Lead Iodides Altered by Chirality of Organic Cations

Po-Jung Huang,[†] Kouji Taniguchi,*[†,‡] and Hitoshi Miyasaka*[†,‡]

† Department of Chemistry, Graduate School of Science, Tohoku University, 6-3 Aramaki-Aza-Aoba, Aoba-ku, Sendai 980-8578, Japan

‡ Institute for Materials Research, Tohoku University, 2-1-1 Katahira, Aoba-ku, Sendai 980-8577, Japan

Supporting Information Placeholder

ABSTRACT: Bulk photovoltaic effect (BPVE) is a promising optoelectronic phenomenon for generating steady-state photocurrent without a bias voltage. Nevertheless, the simple and rational design of materials exhibiting the BPVE remains an important topic in the relevant fields. Here, we report the observation of the BPVE in a simple chiral-polar pair of layered perovskite-type lead iodides in the crystal space group of $P1$ (#1), which were synthesized by assembling R- and S-chiral organic cations, respectively. The sign of the zero-bias photocurrent is altered by the R/S-chirality of the assembled cations, which define the direction of electric polarization derived from the electric dipole moment of each chiral organic cation aligned in a crystal. The strategy of chirality control in a crystal is expected to be useful when searching for BPVE materials.

Noncentrosymmetry brings numerous opportunities for inducing a wide variety of functional characteristics in materials, such as ferroelectricity,[1] piezoelectricity,[1,2] second-harmonic generation,[3,4] circular polarized luminescence,[5,6] Rashba splitting,[7,8] and bulk photovoltaic effect (BPVE).[9,10,11,12,13,14] Among these characteristics, BPVE has been attracting attention as a promising optoelectronic phenomenon for generating steady-state photocurrent without a bias voltage. The conventional photovoltaic effect causes separation of the photo-excited carriers by the built-in electric fields at the heterointerfaces with spatial inhomogeneity such as p-n junctions,[15] whereas that in BPVE is driven by innate crystal asymmetry even in homogeneous materials. Therefore, the BPVE has been mainly investigated in ferroelectric materials.[9,10,11,12,13,14]

On the other hand, given that the BPVE is allowed in noncentrosymmetric materials without an inversion center belonging to 20 point groups (Table S1),[16,17] this effect can be investigated not only in ferroelectric materials but also in general noncentrosymmetric materials. One of the promising approaches for materials design is the chemical introduction of chirality, which definitely breaks the spatial inversion symmetry, into an appropriate system. The chirality-introduced systems should belong to 10 noncentrosymmetric point groups of chiral or chiral-polar point groups in the above-mentioned 20 point groups that allow the BPVE (Table S1). However, the introduction of chirality in pure inorganic systems is very difficult owing to the poor materials designability and processability. Thus, organic-inorganic hybrid materials con-

taining chiral organic species can be potential candidates for the targets in this strategy.[18,19]

In this work, we focused on a class of layered organic-inorganic hybrid perovskite-type (OIHP) lead(II) iodides with a typical formula of $(B)_n(A)_{n-1}Pb_nI_{3n+1}$ as a candidate platform. Monocation A^+ acts as a "perovskitizer" that occupies the central cavity of the corner-sharing PbI_6 octahedra, and monocation B^+ acts as a "spacer" that is confined in the interlayer space of the $[(A)_{n-1}Pb_nI_{3n+1}]^{2-}$ sheets.[20] These OIHP lead(II) iodides possess a merit of high designability in the replacement of organic cations A^+ and B^+, unlike pure inorganic systems.[21,22,23] Similar to the layered lead(II) iodides,[24,25,26] the prototype form $(A)PbI_3$, which is represented as $(MA)PbI_3$ (A^+ = MA^+ = methylammonium ion), is a high-performance photovoltaic material,[27,28] because of the characteristic low trap density for the photo-induced charge carriers in the $[PbI_3]^-$ framework.[29]

Herein, we report the observation of the BPVE under white-light irradiation in chiral-polar OIHP lead(II) iodides synthesized by pre-assembling a chiral cation of $(R)/(S)$-β-methylphenethylammonium ion ($(R)/(S)$-MPA^+) as B^+. The compounds are a pair of R- or S-enantiopure series, (R-$MPA)_2(MA)Pb_2I_7$ (R-1) and $(S$-$MPA)_2(MA)Pb_2I_7$ (S-1). The sign of zero-bias photocurrent is altered depending on the chirality of $(R)/(S)$-MPA^+, which can be associated with the electric polarization produced by the alignment of electric dipole moments in the inserted chiral cations.

Compounds **R-1** and **S-1** are antisymmetrically isostructural and crystallize in the noncentrosymmetric space group of $P1$ (#1) with characteristics of chirality and polarity. The crystal structures of **R-1** and **S-1** are depicted in Figure 1. Along the c-axis direction, these compounds comprise of alternating stacking of double layers of the $(R)/(S)$-MPA^+ layer (B^+ cationic layers as a "spacer") and $[(MA^+)Pb_2I_7]^{2-}$ bilayers ($[(A)_{n-1}Pb_nI_{3n+1}]^{2-}$ anionic layer), where the MA^+ ions are located inside the $[Pb_2I_7]^{3-}$ bilayers and act as a "perovskitizer."[20]

The asymmetric units of **R-1** and **S-1** have crystallographically unique six $(R)/(S)$-MPA^+ and three MA^+ cations. Each $(R)/(S)$-MPA^+ and MA^+ cation possesses a characteristic electric dipole moment, which is caused by partial positive and negative charge distributions in the ammonium and phenyl/alkyl groups of the ionic molecule, respectively. The magnitude of the electric dipole moments of the organic cations, (R)-MPA^+ and MA^+, was evaluated to be 10.773 D (averaged value) and 2.735 D, respectively, by density functional theory (DFT) calculations (Figure S1). These values seem to be significant, in particular for (R)-MPA^+.

However, the values for (*R*)-MPA$^+$ almost cancel out each other when the cations are viewed along the *c** axis (perpendicular to the *ab* plane), reflecting that an average angle of electric dipole moments is 81° to the *ab* plane, whereas that of MA$^+$ is 15° (Figure S2). Consequently, these electric dipole moments of organic cations produce an electric polarization (P_m) approximately along [01̄0] and [010] for *R*-1 and *S*-1, respectively (Figure 2). The P_m value was calculated by the summation of electric dipole moments of each organic cation including *R*-/*S*-MPA and MA per the unit cell volume. The angle between P_m and *b*-axis (/*ab*-plane) is 3.84° (/3.83°). The evaluated magnitude of P_m in the unit cell is 1.06 μC cm^{-2} for *R*-1 (Figure S2), in which the contributions of (*R*)-MPA$^+$ and MA$^+$ in P_m are 0.54 μC cm^{-2} and 0.52 μC cm^{-2}, respectively. The evaluated P_m value is comparable with those reported for ferroelectric layered OIHP lead(II) halides.[30,31,32,33] The sign reversal of P_m between *R*-1 and *S*-1 (Figure 2) reflects the symmetry constraint of the chiral-polar system. Because the structures of the enantiomers are converted by an inversion operation with a combination of mirror and two-fold rotation operations in the chiral-polar system, the electric polarization is simultaneously reversed between the enantiomers (Figure S3).
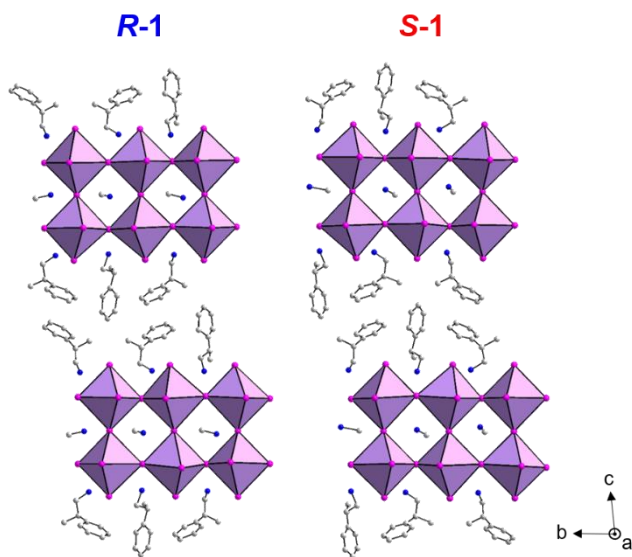

Figure 2. Perspective views perpendicular to the Pb−I bilayers (along the *c**-axis) for *R*-1 and *S*-1. The small green arrows represent the summation of calculated electric dipole moments of one MA$^+$ and two MPA$^+$ projected on the *ab* plane. The large green arrows represent the electric polarization originated from organic molecule cations in the *ab* plane. The organic components are omitted for clarity.

Figure 1. Crystal structure of *R*-1 and *S*-1 along [100] with color codes Pb (lavender), I (pink), C (gray), N (blue). The PbI$_6$-units are displayed as polyhedra, and H atoms are omitted for clarity.

Regarding the inorganic part (the [Pb$_2$I$_7$]$^{3-}$ bilayer) of the crystal structure, two types of Pb–I bonds are defined: 1) axially directional Pb–I bonds (i.e., stacking direction), which are nearly vertical to the [Pb$_2$I$_7$]$^{3-}$ bilayer, and 2) equatorially directional Pb–I bonds, constructing the layer framework (Figure S4).

An optical absorption spectrum of *R*-1 measured using a KI pellet is shown in Figure 3. The absorption spectrum displays several absorption peaks in the ultraviolet-visible (UV-VIS) light region. The Tauc plot, (Ahv)^2 vs. energy with the absorbance *A*, estimates a band gap of ~2.08 eV (inset of Figure 3).[34] This can allow a direct transition, as shown in this type of perovskite-type lead(II) halide materials.[30] The circular dichroism spectra for both enantiomers were measured using thin film technique (Figure S5).[35]
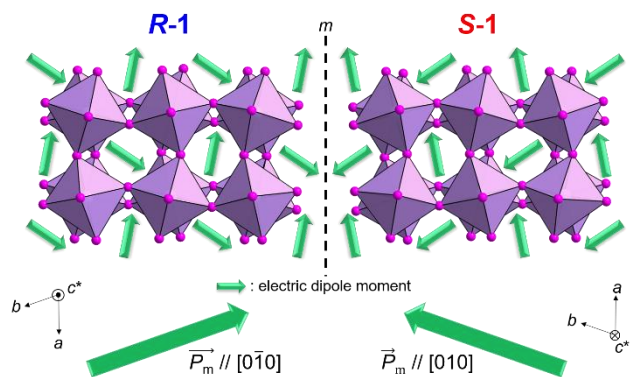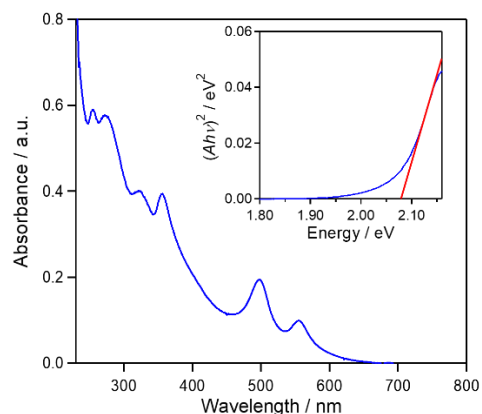

Figure 3. An optical absorption spectrum of *R*-1 measured using a KI pellet. Inset: (Ahv)^2 versus energy (Tauc plot) with red solid line intercept representing a band gap of approximately 2.08 eV.

The voltage dependence of current (*I−V* curve) was measured on a single crystal for both *R*-1 and *S*-1 between external potentials of ± 1 V (Figure S6). First, the electrodes were attached to the [010] direction of the single crystal, which was parallel to the positive direction of the electric field (Figures 4(a) and S7). Under white-light irradiation with a power of 16 kW m^{-2}, the currents of *R*-1 and *S*-1 increased by approximately three orders of magnitude from 5 pA and 10 pA in the dark to 1.96 nA and 2.93 nA at 1 V, respectively (Figure S6). The light-wavelength dependence of *I−V* curves was observed at several wavelengths from 400 nm to 730 nm by changing band-path filters (Figure S8). This analysis revealed a clear light-wavelength-dependent variation at a shorter wavelength just below 600 nm (2.07 eV). This trend indicates that the photo-excited carriers are generated by higher energies beyond the band gap (~2.08 eV).

The BPVE was clearly observed in the *I−V* curve for the [010] parallel alignment with a zero-bias photocurrent, which is a current detected at 0 V, |I_0| ~ 0.1 nA, and an open circuit voltage, |V_0| ~ 50 mV, for both *R*-1 and *S*-1 (Figure 4(a)). The magnitude of the detected I_0 is comparable to that reported in the ferroelectric layered OIHP lead(II) halides.[31] Although we conducted the *I−V* measurement also for the racemic compound (**rac-1**), the BPVE was not observed (Figures 4(a) and 4(b)). Notably, the BPVE depends on the P_m of the materials, namely the signs (±) of I_0 and

V_0 are inverse between **R-1** and **S-1** with opposite P_m (Figure 4(a)): $I_0 < 0$ and $V_0 > 0$ for **R-1** and $I_0 > 0$, $V_0 < 0$ for **S-1**. These sign assignments of I_0 and V_0 were checked in the four devices for each enantiomer, and one of the data sets is shown in Figure S9. In addition, the reproducibility of the BPVE was assessed by repeating white-light irradiation on the samples, where repeatable switching of the zero-bias photocurrent was observed for at least four cycles (Figure S10). To elucidate the correlation with P_m in BPVE, the P_m-perpendicular directional photocurrent, in which the electrodes were attached to the perpendicular to [010] in the *ab* plane of the crystal, was measured for both crystals of **R-1** and **S-1** (Figures 4(b) and S11). In this configuration, I_0 and V_0 were no longer detected (Figure 4(b)), indicating that the BPVE is associated with polarity along [010] in **R-1** and **S-1**. However, the signs of I_0 and V_0 are opposite from those predicted from the internal electric field produced by P_m. Here, considering that the P_m is a partial electric polarization generating only from the organic molecule cations, one possible scenario is that the direction of total electric polarization, which consists of electric dipole moments produced by the charge distribution of both the inorganic layers and organic molecule cations, could be almost antiparallel to P_m in the *ab* plane. From the materials design viewpoint, although the BPVE in **R-1** and **S-1** are dominated by polarity, it should be noted that the BPVE is tunable by selecting chiral components in the synthetic procedure through correlation between polarity and chirality in a chiral-polar system.
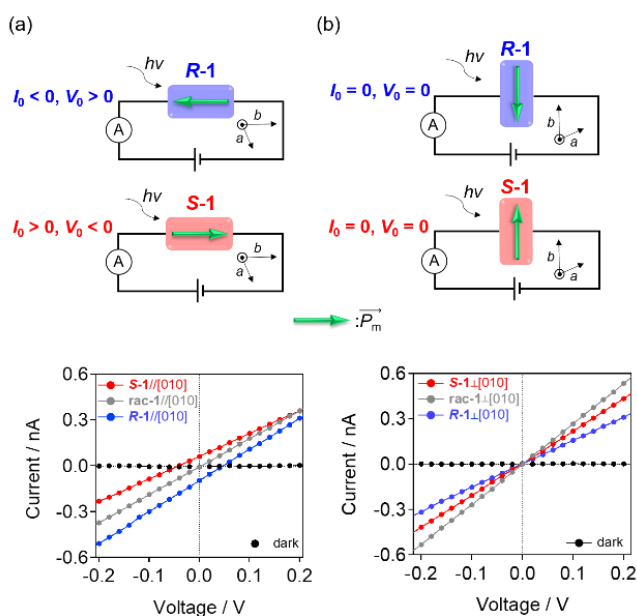

Figure 4. Schematic views of the photocurrent measurement configuration for single-crystals of **R-1** and **S-1**. [010]-axis is placed ((a) top) parallel and ((b) top) vertical to the direction of the applied electric field. The P_m is displayed by the green arrows. The expanded views of *I−V* curves near 0 V measured with irradiation (blue, red, and gray circles and lines) and without irradiation (black circles and lines) of simulated solar white-light, which was measured in ((a) bottom) parallel and ((b) bottom) perpendicular configurations between [010] and the applied electric field.

In summary, we have successfully demonstrated the BPVE in an enantiomer set of noncentrosymmetric layered OIHP lead(II) iodides, in which chiral cations were rationally introduced to break the spatial inversion symmetry. The sign of the zero-bias photocurrent, which originates from the photovoltaic effect, depends on the direction of electric polarization, which is produced by the alignment of electric dipole moments in the inserted chiral organic cations. Although the polarity is consequently crucial, this

work indicates that the introduction of chiral groups in the system is useful for the design of BPVE materials in the case that the correlation present between chirality and polarity. This work shows the potential of OIHP systems as material-tailoring platforms for realizing novel functionalities induced by spatial inversion symmetry breaking.

ASSOCIATED CONTENT

Supporting Information

Experimental section, results of the DFT calculation (Figures S1 and S2), structural information (Figures S3, S4 and Table S2), CD spectra (Figure S5), *I−V* curves (Figures S6, S8, S9a, and S9b), reproducibility of BPVE (Figure S10), PXRD patterns (Figure S12), the *I−V* curves-measurement configuration (Figures S7, S9c−S9f, S11, and S13) and symmetry information (Table S1). The Supporting Information is available free of charge on the ACS Publications website. brief description (file type, i.e., PDF)

AUTHOR INFORMATION

Corresponding Author

*E-mail for K.T.: taniguchi@imr.tohoku.ac.jp, H.M.: miyasaka@imr.tohoku.ac.jp

Notes

The authors declare no competing financial interest.

REFERENCES

1   Scott, J. F., Applications of modern ferroelectrics. *Science* **2007**, *315*, 954–959.

2   Rodel, J.; Jo, W.; Seifert, K. T. P.; Anton, E. M.; Granzow, T.; Damjanovic, D., Perspective on the development of lead-free piezoceramics. *J. Am. Ceram. Soc.* **2009**, *92* 1153–1177.

3   Wang, C.; Zhang, T.; Lin, W., Rational synthesis of noncentrosymmetric metalorganic frameworks for second-order nonlinear optics. *Chem. Rev.* **2012**, *112*, 1084–1104.

4   Verbiest, T.; Elshocht, S. V.; Kauranen, M.; Hellemans, L.; Snauwaert, J.; Nuckolls, C.; Katz, T. J.; Persons, A. Strong enhancement of nonlinear optical properties through supramolecular chirality. *Science* **1998**, *282*, 913–915.

5   Carr, R.; Evans, N. H.; Parker, D., Lanthanide complexes as chiral probes exploiting circularly polarized luminescence. *Chem. Soc. Rev.* **2012**, *41*, 7673–7686.

6   Lunkley, J. L.; Shirotani, D.; Yamanari, K.; Kaizaki, S.; Muller, G. Extraordinary circular polarized luminescence activity exhibited by cesium tetakis(3-heptafluoro-butylryl-(+)-camphorato) Eu(III) complexes in EtOH and $CHCl_3$ solutions. *J. Am. Chem. Soc.* **2008**, *130*, 13814–13815.

7   Rashba, E. I., Properties of semiconductors with an extremum loop. 1. cyclotron and combinational resonance in a magnetic field perpendicular to the plane of the loop. *Sov. Phys. Solid State* **1960**, *2*, 1109–1122.

8   Ishizaka, K.; Bahramy, M. S.; Murakawa, H.; Sakano, M.; Shimojima, T.; Sonobe, T.; Koizumi, K.; Shin, S.; Miyahara, H.; Kimura, A.; Miyamoto, K.; Okuda, T.; Namatame, H.; Taniguchi,

M.; Arita, R.; Nagaosa, N.; Kobayashi, K.; Murakami, Y.; Kumai, R.; Kaneko, Y.; Onose, Y.; Tokura, Y., Giant Rashba-type spin splitting in bulk BiTeI. *Nat. Mater.* **2011**, *10*, 521–526.

9 Butler, K. T.; Frost, J. M.; Walsh, A., Ferroelectric materials for solar energy conversion: photoferroics revisited. *Energy. Environ. Sci.* **2015**, *8*, 838–848.

10 Glass, A. M.; von der Linde, D.; Negran, T. J. High-voltage bulk photovoltaic effect and the photorefractive process in $LiNbO_3$. *Appl. Phys. Lett.* **1974**, *25*, 233–235.

11 Yang, S.Y.; Seidel, J.; Byrnes, S. J.; Shafer, P.; Yang, C.-H.; Rossell, M. D.; Yu, P.; Chu, Y.-H., Scott, J. F.; Ager, J. W.; Martin, L. W.; Ramesh, R., Above-bandgap voltage from ferroelectric photovoltaic devices. *Nat. Nanotechnol.* **2010**, *5*, 143–147

12 Grinberg, I.; West, D. V.; Torres, M.; Gou, G.; Stein, D. M.; Wu, L.; Chen, G.; Gallo, E. M.; Akbashev, A. R.; Davies, P. K.; Spanier, J. E.; Rappe, A. M., Perovskite oxides for visible-light-absorbing ferroelectric and photovoltaic materials. *Nature* **2013**, *503*, 509–512.

13 Nechache, R.; Harnagea, C.; Li, S.; Cardenas, L.; Huang, W.; Chakrabartty, J.; Rosei, F., Bandgap tuning of multiferroic oxide solar cells. *Nat. Photonics* **2015**, *9*, 61–67.

14 Nakamura, M.; Horiuchi, S.; Kagawa, F.; Ogawa, N.; Kurumaji, T.; Tokura, Y.; Kawasaki, M., Shift current photovoltaic effect in a ferroelectric charge-transfer complex. *Nat. Commun.* **2017**, *8*, 281.

15 Shockley, W.; Queisser, H. J., Detailed balance limit of efficiency of *p-n* junction solar cells. *J. Appl. Phys.* **1961**, *32*, 510–519.

16 Baltz, R.; Kraut, W., Theory of the photovoltaic effect in pure crystals. *Phys. Rev. B* **1981**, *23*, 5590–5596.

17 Spanier, J. E.; Fridkin, V. M.; Rappe, A. M.; Akbashev, A. R.; Polemi, A.; Qi, Y.; Gu, Z.; Young, S. M.; Hawley, C. J.; Imbrenda, D.; Xiao, G.; Bennett-Jackson, A. L.; Johnson, C. L., Power conversion efficiency exceeding the Shockley-Queisser limit in a ferroelectric insulator. *Nat. Photonics* **2016**, *10*, 611–616.

18 Long, G.; Jiang, C.; Sabatini, R.; Yang, Z.; Wei, M.; Quan, L. N.; Liang, Q.; Rasmita, A.; Askerka, M.; Walters, G.; Gong, X.; Xing, J.; Wen, X.; Quintero-Bermudez, R.; Yuan, H.; Xing, G.; Wang, X. R.; Song, D.; Voznyy, O.; Zhang, M.; Hoogland, S.; Gao, W.; Xiong, Q.; Sargent, E. H., Spin control in reduced-dimensional chiral perovskites. *Nat. Photonics* **2018**, *12*, 528–533.

19 Long, G.; Zhou, Y.; Zhang, M.; Sabatini, R.; Rasmita, A.; Huang, L.; Lakhwani, G.; Gao, W., Theoretical prediction of chiral 3D hybrid organic-inorganic perovskites. *Adv. Mater.* **2019**, *31*, 1807628.

20 Stoumpos, C. C.; Mao, L.; Malliakas, C. D.; Kanatzidis, M. G., Structure-band gap relationships in hexagonal polytypes and low-dimensional structures of hybrid tin iodide perovskites. *Inorg. Chem.* **2017**, *56*, 56–73.

21 Yang, C.-K.; Chen, W.-N.; Ding, Y.-T.; Wang, J.; Rao, Y.; Liao, W.-Q.; Tang, Y.-Y.; Li, P.-F.; Wang, Z.-X.; Xiong, R.-G., The first 2D homochiral lead iodide perovskite ferroelectrics: [*R*- and *S*-1-(4-chlorophenyl)ethylammonium]$_2PbI_4$. *Adv. Mater.* **2019**, *31*, 1808088.

22 Chen, C.; Gao, L.; Gao, W.; Ge, C.; Du, X.; Li, Z.; Yang, Y.; Niu, G.; Tang, J., Circularly polarized light detection using chiral hybrid perovskite. *Nat. Commun.* **2019**, *10*, 1927.

23 Ma, J.; Fang, C.; Chen, C.; Jin, L.; Wang, J.; Wang, S.; Tang, J.; Li, D., Chiral 2D perovskites with a high degree of circularly polarized photoluminescence. *ACS Nano* **2019**, *13*, 3659–3665.

24 Tsai, H.; Nie, W.; Blancon, J.-C.; Soumpos, C. C.; Asadpour, R.; Harutyunyan, B.; Neukrich, A. J.; Verduzco, R.; Crochet, J. J.; Tretiak, S.; Pedesseau, L.; Even J.; Alam, M. A.; Gupta, G.; Lou, J.; Ajayan, P. M.; Bedzyk, M. J.; Kanatzidis, M. G.; Mohite, A. D., High-efficiency two-dimensional Ruddlesden-Popper perovskite solar cells. *Nature* **2016**, *536*, 312–316.

25 Mao, L.; Stoumpos, C. C.; Kanatzidis, Two-dimensional hybrid halide perovskites; principles and promises, *J. Am. Chem. Soc.* **2019**, *141*, 1171–1190.

26 Quintero-Bermudez, R.; Gold-Parker, A.; Proppe, A. H.; Munir, R.; Yang, Z.; Kelley, S. O.; Amassian, A.; Toney, M. F.; Sagent, E. H. Compositional and orientational control in metal halide perovskites of reduced dimensionality. *Nat. Mater.* **2018**, *17*, 900–907.

27 Kojima, A.; Teshima, K.; Shirai, Y.; Miyasaka, T., Organometal halide perovskites as visible-light sensitizers for photovoltaic cells. *J. Am. Chem. Soc.* **2009**, *131*, 6050–6051.

28 Burschka, J.; Pellet, N.; Moon, S.-J.; Humphry-Baker, R.; Gao, P.; Nazeeruddin, M. K.; Grätzel, M., Sequential deposition as a route to high-performance perovskite-sensitized solar cells. *Nature* **2013**, *499*, 316–319.

29 Shi, D.; Adinolfi, V.; Comin, R.; Yuan, M.; Alarousu, E.; Buin, A.; Chen, Y.; Hoogland, S.; Rothenberger, A.; Katsiev, K.; Losovyj, Y.; Zhang, X.; Dowben ,P. A.; Mohammed, O. F.; Sargent, E. H.; Bakr O. M., Low trap-state density and long carrier diffusion in organolead trihalide perovskite single crystals. *Science* **2015**, *347*, 519–522.

30 Liao, W.-Q.; Zhang, Y.; Hu, C.-L.; Mao, J.-G.; Ye, H.-Y.; Li, P.-F.; Huang, S. D.; Xiong, R.-G., A lead-halide perovskite molecular ferroelectric semiconductor. *Nat. Commun.* **2015**, *6*, 7338.

31 Sun, Z.; Liu, X.; Khan, T.; Ji, C.; Asghar, M. A.; Zhao, S.; Li, L.; Hong, M.; Luo, J., A photoferroelectric perovskite-type organometallic halide with exceptional anisotropy of bulk photovoltaic effects. *Angew. Chem. Int. Ed.* **2016**, *55*, 6545–6550.

32 Li, L.; Sun, Z.; Wang, P.; Hu, W.; Wang, S.; Ji, C.; Hong, M.; Luo, J., Tailored engineering of an unusual $(C_4H_9NH_3)_2(CH_3NH_3)_2Pb_3Br_{10}$ two-dimensional multilayered perovskite ferroelectric for a high-performance photodetector. *Angew. Chem. Int. Ed.* **2017**, *56*, 12150–12154.

33 Li, L.; Shang, X.; Wang, S.; Dong, N.; Ji, C.; Chen, X.; Zhao, S.; Wang, J.; Sun, Z.; Hong, M.; Luo, J., Bilayered hybrid perovskite ferroelectric with giant two-photon absorption. *J. Am. Chem. Soc.* **2018**, *140*, 6806–6809.

34 Tauc, J., Optical properties and electronic structure of amorphous Ge and Si. *Mater. Res. Bull.* **1968**, *3*, 37–46.

35 Ahn, J.; Lee, E.; Tan, J.; Yang, W.; Kim, B.; Moon, J., A new class of chiral semiconductors: chiral-organic-molecule-incorporating organic-inorganic hybrid perovskites. *Mater. Horiz.* **2017**, *4*, 851–856.

TOC